

Exciting Dilute Magnetic Semiconductor: Copper-Doped ZnO

S. Karamat · R.S. Rawat · T.L. Tan · P. Lee ·
S.V. Springham · Anis-ur-Rehman · R. Chen · H.D. Sun

Received: 28 April 2012 / Accepted: 25 June 2012 / Published online: 22 July 2012
© Springer Science+Business Media, LLC 2012

Abstract The present study is focused on the copper-doped ZnO system. Bulk copper-doped ZnO pellets were synthesized by a solid-state reaction technique and used as target material in pulsed laser deposition. Thin films were grown for different Cu doped pellets on sapphire substrates in vacuum (5×10^{-5} mbar). Thin films having (002) plane of ZnO showed different oxidation states of dopants. $M-H$ curves exhibited weak ferromagnetic signal for 1–3 % Cu doping but for 5 % Cu doped thin film sample showed the diamagnetic behavior. For deeper information, thin films were grown for 5 % Cu doped ZnO bulk pellet in different oxygen ambient pressures and analyzed. PL measurement at low temperature showed the emission peak in thin films samples due to acceptor-related transitions. XPS results show that copper exists in Cu^{2+} and Cu^{+1} valence states in thin films and with increasing O_2 ambient pressure the valence-band maximum in films shifts towards higher binding energy. Furthermore, in lower oxygen ambient pressure (1×10^{-2} mbar) thin films showed magnetic behavior but this vanished for the film grown at higher ambient pressures of oxygen (6×10^{-2} mbar), which hints towards the decrease in donor defects.

Keywords Thin films · Dilute magnetic semiconductor

1 Introduction

From last few years, rapid efforts are in progress toward spintronics technology, where the charge and spin degree of freedom, both can be utilized in electronic devices. It is believed that spintronics devices will be higher in speed, efficient and having less consumption of power [1]. Dilute magnetic semiconductors (DMSs) are the stronger candidates in the realm of spintronics. Metallic-based spintronics devices have become a substantial part of the today electronics. The ground breaking discovery in spintronics developments started from the discovery of giant magnetoresistance effect observed in multilayered magnetic materials [2, 3]. In order to meet the demands of society, several spintronics devices need to be developed, where the existing issues should be resolved. In computing technology where information processing is based on spins as the data carriers, it is necessary that a device must have a component which produces spin polarized carriers and has reliable transport in it. It means that a device should have ferromagnetic materials which help in the electron spin storage and a semiconductor material as well which would perform traditional device operation. It looks easy to develop a device which contains ferromagnetic and semiconductor material together. Even so, the conductivities between two materials should be matched closely for efficient injection of spin polarized carriers into the semiconductor part [4], like metal-metal junctions [5]. In case of large difference between the materials conductivity, the degree of spin polarization will be reduced in semiconductors. To achieve high degree of spin polarization from ferromagnetic part, it is essential that the conductivities of

S. Karamat (✉) · R.S. Rawat · T.L. Tan · P. Lee · S.V. Springham
Natural Science and Science Education, National Institute
of Education, Nanyang Technological University,
Singapore 637616, Singapore
e-mail: shumailakaramat@gmail.com

S. Karamat · Anis-ur-Rehman
Department of Physics, COMSATS Institute of Information
Technology, 22060 Islamabad, Pakistan

R. Chen · H.D. Sun
Division of Physics and Applied Physics, School of Physical &
Mathematical Sciences, Nanyang Technological University,
Singapore 637371, Singapore

both materials should be matched closely. Both of these solutions can be achieved easily in a heterostructure device having ferromagnetic metal-semiconductor junction having 100 % spin polarization from ferromagnetic metal to semiconductor [6]. DMSs are excellent candidates in resolving these issues because the presence of magnetic impurities in semiconducting host lattice will be the source of spin polarized carriers giving a new approach of spin injection. By utilizing DMSs, the difficulty of conductivity mismatching at the interfacial layer of metal and semiconductor materials would be removed [7]. However, many DMSs become unsuccessful due to a low Curie temperature (less than room temperature), hindering their practical applications. A lot of research is still going on in order to achieve DMSs whose Curie temperature will be higher than room temperature to make their utility feasible in devices. Transition metal-doped wide band gap DMS materials have the capacity to show Curie temperature at and above room temperature and a lot of researchers focused their attention on these materials.

The present paper is on the study of copper-doped ZnO thin films using pulsed laser deposition (PLD). Copper-doped ZnO is of interest because metallic copper and its oxides (Cu_2O , CuO) are not magnetic in nature, which increases the chances of DMS which has ferromagnetism only due to doping. Different reports showed contradictory results about the nature of the copper-doped ZnO system, it gives us motivation to gain deeper insight in the system by detailed structural and compositional analysis.

2 Experiments

Thin films were grown by PLD from $(\text{ZnO})_{1-x}(\text{CuO})_x(\text{Al}_2\text{O}_3)_{0.002}$ with $x \leq 0.05$ series of targets. The PLD targets were made from the powders copper oxide (CuO) and zinc oxide (ZnO) powder with 0.2 % Al_2O_3 addition. CuO powder of different percentage (1–5 %) was mixed with host ZnO according to the required stoichiometric values. This combined powder was mixed and ball milled. After milling for 16 hrs, powders were calcined for 14 hrs at 400 °C. Calcined powders of $(\text{ZnO})_{1-x}(\text{CuO})_x(\text{Al}_2\text{O}_3)_{0.002}$ were compressed to form pellets of 25 mm diameter and further sintered at 1200 °C for 16 hrs. After detailed structural, compositional, magnetic characterization of bulk samples, they were used as a PLD target in pulsed laser deposition systems. Nd:YAG laser ($\lambda = 532$ nm) having 10 Hz repetition rate was used to ablate copper-doped ZnO targets. Different numbers of laser shots were used to grow films in vacuum (5×10^{-5} mbar), and O_2 ambience. The film thickness was analyzed by a profile meter. The study of the crystallographic structures of the pellets and thin films was performed using a X-ray diffractometer. The electronic states of elements and compositional % of Zn, O and Cu, were estimated by XPS for bulk and thin film samples. The structural

information of the ZnCuO system was also obtained from their vibrational modes using Renishaw Raman spectrophotometer. He–Ne laser (632 nm) was used for excitation and the incident laser power was 40 mW. Magnetic measurements were performed for bulk and thin films using VSM at room temperature. Photoluminescence (PL) spectroscopy of thin films were done to get knowledge about different emissions. The electron carrier density in thin films was investigated by Hall effect measurement.

2.1 Results and Discussions

Figure 1(a) shows the XRD spectra of the copper-doped ZnO bulk samples. XRD patterns for all bulk samples consist of peaks corresponding to ZnO (host lattice), with the absence of any secondary or impurity phase. The Rietveld refinement was done for some samples to get an idea about the change in lattice parameters due to copper ion substitution. Information about a and c , lattice parameters of bulk samples were obtained by Rietveld quantifications, which showed difference from the standard values of ICSD-26170 ZnO lattice parameters. Lattice parameter $a = 3.2510$ Å obtained from Rietveld refinements giving 0.0021 Å increase from the standard value (3.2489 Å), while the lattice parameter $c = 5.2031$ Å shows a decrease of 0.0018 Å from the standard value (5.2049 Å). Substitution of Cu ion into ZnO causes a change in lattice spacing.

Information about composition of Cu doped ZnO bulk pellets was obtained from X-ray photoelectron spectroscopy (XPS). For greater accuracy in compositional analysis, the elemental compositions were measured on the surface and beneath the surface (after etching) of the bulk samples. Survey scans of pellets' surface showed the presence of different elements: zinc, copper, oxygen, carbon, aluminum. To get unambiguous information, pellets' surface was etched up to 100 nm, which removes the peak corresponding to carbon appearing at surface. XPS results of etched pellets are shown here for reliable analysis. XPS scans for Zn and Cu 2p core peaks are shown in Fig. 1(b) and 1(c). For all Cu doping percentages the Zn 2p core peak, refer to Fig. 1(b), showed symmetrical trend in binding energy (BE). Zn 2p_{3/2} peaks having BE around 1020.4 ± 0.1 eV, showing a variation of 0.9 ± 0.1 eV from the reported of ZnO (1021.4 eV) [8]. Copper substitution may cause the shift in BE value. Figure 1(c) shows Cu 2p core peaks spectrum for same compositions. Core peak scan gives Cu 2p_{3/2} and Cu 2p_{1/2} BE value around 931.9 ± 0.3 eV and 951.7 ± 0.3 eV, respectively, for all pellets, giving information about +2 oxidation state of Cu ions [9]. Cu^{+2} ions have the capacity to substitute successfully the Zn^{+2} ion in ZnO lattice which means the existence of ZnCuO phase, and the magnetic moments of doping Cu contribute as a source of magnetism in the samples.

Fig. 1 (a) X-ray diffraction spectrum for $(\text{ZnO})_{1-x}(\text{CuO})_x(\text{Al}_2\text{O}_3)_{0.002}$ pellets for $x \leq 0.05$. (b) Zn 2p core peaks obtained from XPS for $(\text{ZnO})_{1-x}(\text{CuO})_x(\text{Al}_2\text{O}_3)_{0.002}$ pellets for $(x \leq 0.05)$. (c) Cu 2p core peaks obtained from XPS for $(\text{ZnO})_{1-x}(\text{CuO})_x(\text{Al}_2\text{O}_3)_{0.002}$ pellets for $(x \leq 0.05)$

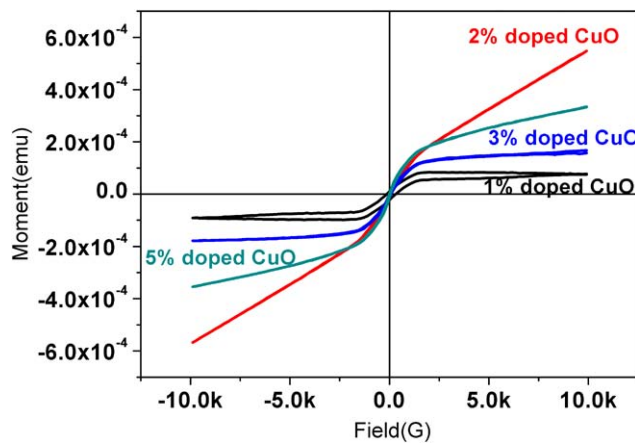
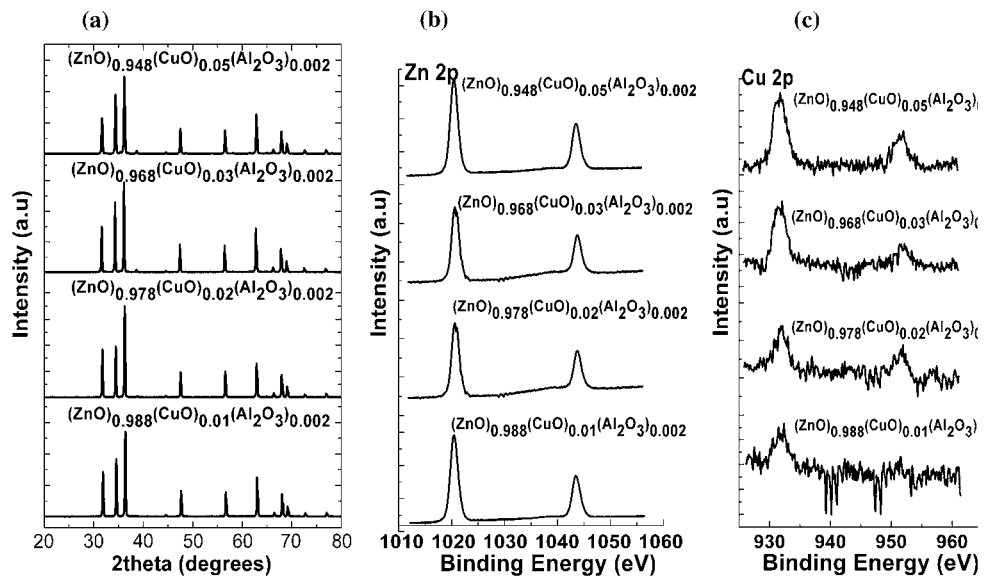


Fig. 2 $M-H$ curves for $(\text{ZnO})_{1-x}(\text{CuO})_x(\text{Al}_2\text{O}_3)_{0.002}$ bulk samples

VSM was used to get information about magnetic behavior of samples at room temperature. $M-H$ loops for all bulk pellets are shown in Fig. 2. The shape of hysteresis curve indicates weak ferromagnetism in samples. It is believed that ferromagnetic interactions arise in bulk samples due to substitution of Cu^{2+} ions in ZnO host lattice. Oxidation state of Cu^{2+} ions, which is +2, was measured by XPS. There are few reports which showed that ferromagnetic behavior in copper-doped ZnO system is dependent on doping percentage, the less the doping quantity, the more ferromagnetic behavior [9], and results shown in Fig. 2 also support this reason.

Bulk pellets after their characterizations were further utilized as a PLD target and thin films were deposited from them under different conditions. Thin films were deposited using 9000 laser shots in vacuum environment at 5×10^{-6} mbar background ambient pressure. XRD graphs shown in Fig. 3 exhibiting strong (002) reflection peak of

ZnO appear about $2\theta = 34.4^\circ$ along with another weak peak at about 72° corresponding (004) plane for all the thin film samples grown on sapphire substrates with varying Cu doping concentration. The observation of diffraction peaks corresponding to the same (00l) family indicates good texture with the c -plane of the sapphire substrates for all the samples. The appearance of (00l) family of peaks shows only one orientation in thin films. The average crystallite sizes were calculated using Scherrer's equation for (002) diffraction plane of thin films deposited on sapphire substrates [10, 11]. The average crystallite sizes are in narrow range of 16 to 20 nm, shown in Fig. 3, inset, indicating thereby nanophase thin film growth.

Information about surface composition of thin films was obtained by XPS. High resolution scan of Cu 2p core peaks was measured for all samples, Cu 2p doublet of Cu $2p_{3/2}$ and Cu $2p_{1/2}$ peaks appearing in all samples. BE value for Cu 2p core peaks of all samples show asymmetrical trend. The presence of different oxidation states of the element may be the cause of asymmetrical behavior. In order to understand asymmetrical trend in BE and to verify the existence of various possible oxidation states, core peak spectra of Cu 2p for all samples were deconvoluted-not shown here. The appearance of peaks having BE at 931.5 ± 0.4 and 933.0 ± 0.4 eV is reason to propose mixed valence state of +1 and +2 charge of Cu, in which +2 is dominant oxidation state. The electronic configuration of Cu^{2+} is $3d^9 4s^0$ and that of Cu^{1+} is $3d^{10} 4s^0$. It is well known that Cu existing in the +1 oxidation state has no unpaired spins so there is no ferromagnetic contribution; while Cu ion having +2 state has unpaired spins exhibiting net magnetic moment and can contribute to ferromagnetic behavior. It is expected that the thin film samples grown in high vacuum conditions may exhibit ferromagnetic behavior because of the +2 oxidation state of Cu [12, 13]. O1s core peak spectrum, also

not shown here, exhibits asymmetrical trends in BE. The presence of multi-component oxygen species is the reason of asymmetry in oxygen BE values. In summary, a detailed XPS analysis of films indicates different oxidation states of dopants, of which the dominant state is +2, which is the expected cause of ferromagnetic behavior in thin film samples.

$M-H$ measurements were done using VSM at room temperature for all thin film samples. magnetic background of

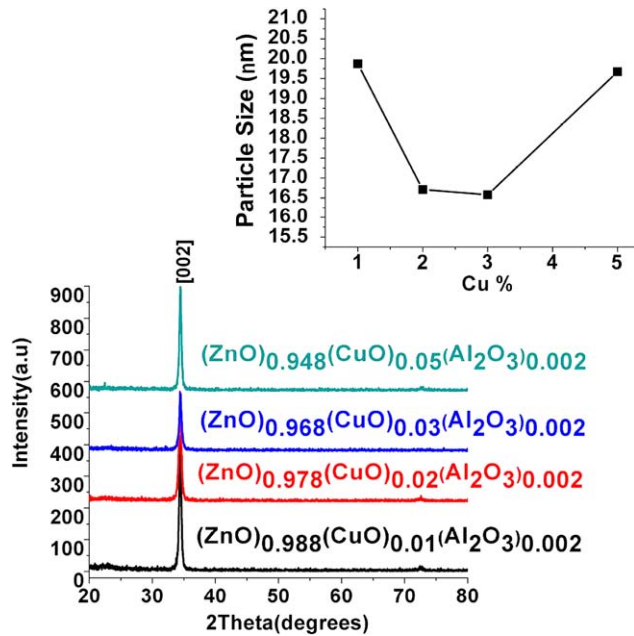


Fig. 3 XRD graphs for thin films grown on Sapphire substrates at 5×10^{-5} mbar. Inset shows average crystallite size for the thin films grown on sapphire substrates

substrates was done for all samples. Film samples grown in vacuum with 1 to 3 % doping are found to be weakly ferromagnetic, while the 5 % doping sample exhibits diamagnetic behavior, shown in Fig. 4. Thin films grown from 5 % Cu doped ZnO pellet give diamagnetic curve in vacuum deposition, motivating us for further investigation to see whether the thin film growth at certain oxygen partial pressure can promote the ferromagnetic behavior in these thin films.

XRD spectra for films deposited at 750 °C using $(\text{ZnO})_{0.948}(\text{CuO})_{0.05}(\text{Al}_2\text{O}_3)_{0.002}$ pellet, in different oxygen pressures, are shown in Fig. 5(a).

It is observed that for all the XRD patterns of thin films, shown in Fig. 5(a), only (002) and (004) reflections are present at $2\theta = 34.44^\circ$ and 72.56° , respectively. XRD diffraction patterns of highly textured thin films clearly indicate that at very early stages thin films achieved the preferred growth orientation. It was reported that the reason of preferred orientation can be of chemical nature rather than crystallographic. The main idea of this statement is based on the opposition between Zn atoms and O atoms of the ZnO while the attraction between bonded Zn atoms towards oxygen atoms is present on substrate surface. It favors greater population of two-dimensional Zn atoms along (002) plane of wurtzite structure, and films grow along these orientations [14]. On crystallographic basis, the surface energy of ZnO crystal becomes minimum along (002) orientation, it helps the growth of c -axis oriented ZnO crystal. It was reported that growth of ZnO along c -axis can be done at lower oxygen pressure (0.013 mbar) [15]. In our case, lower oxygen partial pressure (e.g. 1×10^{-2} – 6×10^{-2} mbar) was used and a minimum effect in (002) peak width was observed for

Fig. 4 $M-H$ curves for thin film samples

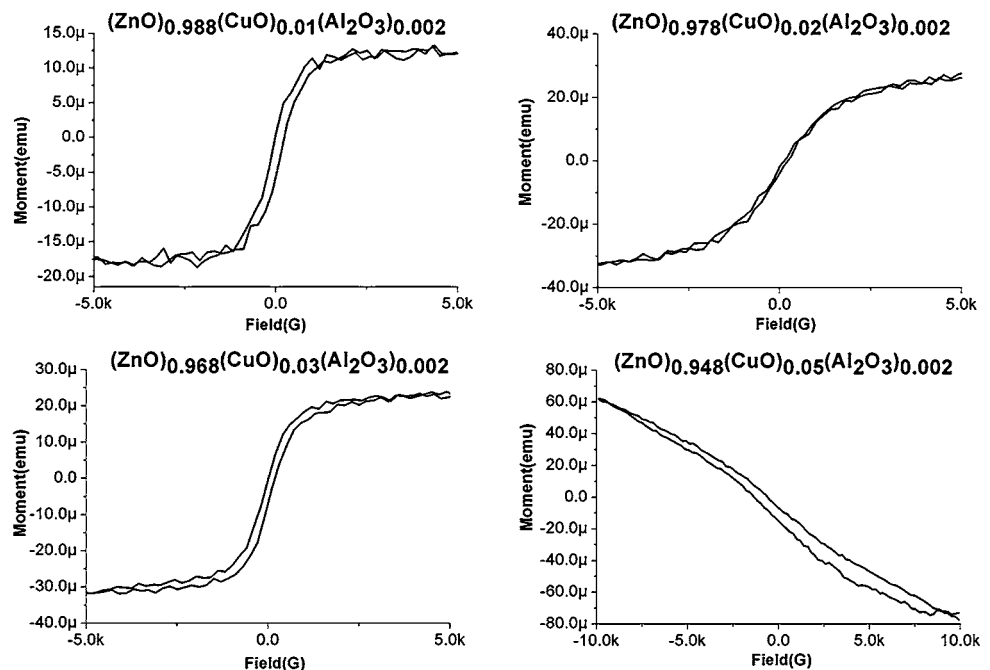


Fig. 5 (a) XRD spectra for thin films grown in oxygen ambient pressures at 750 °C. (b) PL spectra of $(\text{ZnO})_{1-x}(\text{CuO})_x(\text{Al}_2\text{O}_3)_{0.002}$ thin films grown in different oxygen pressures

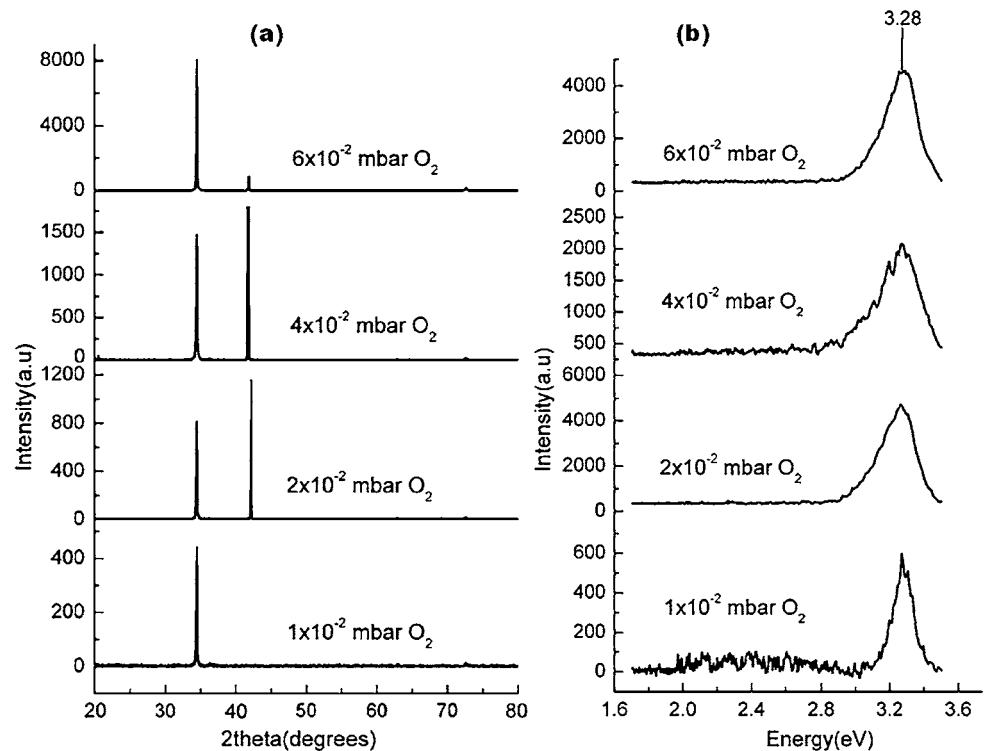


Table 1 Crystallite size and dislocation density for (002) peak of thin films

O ₂ pressure	2θ for (002) reflection (degree)	Crystallite size (nm)	Dislocation density (Å ⁻²)
1 × 10 ⁻² mbar	34.44	56.04	3.18 × 10 ⁻⁶
2 × 10 ⁻² mbar	34.44	60.04	2.77 × 10 ⁻⁶
4 × 10 ⁻² mbar	34.45	52.54	3.62 × 10 ⁻⁶
6 × 10 ⁻² mbar	34.45	70.05	2.03 × 10 ⁻⁶

ZnCuO thin films. In order to obtain more information about structural properties, average crystallite size (*D*) (using the Scherrer formula) along dislocation density (*δ*) was calculated for preferred orientations of thin films [10, 11, 16–18]. The higher the *δ* values the lower will be the crystalline levels in films, dislocation density values give the number of defects in thin films. Average crystallite size, dislocation density, change in peak width of preferred orientation for thin films grown at different oxygen partial pressures are given in Table 1. These values are comparative to other reported work [16].

The most valuable information on the quality of the films may be obtained by PL measurements. Photoluminescence (PL) spectroscopy was used to get information about the change in luminescence due to Cu doping in ZnO and different oxygen ambient pressure during thin films growth, shown in Fig. 5(b). Near band edge (NBE) emission was observed at about 3.27 eV (~380 nm) for thin film samples.

Wang’s group showed that NBE emission peaks become intense with the increasing Cu concentration, NBE peak intensity depends strongly on Cu. They observed increase in NBE for 2 at.% Cu atoms doped in ZnO as undoped ZnO film samples. Exciton related recombination is the cause of NBE emissions in materials [20, 21]. In our case, thin films grown in increasing oxygen ambient pressure show an increase in ultra-violet (UV) luminescence observed in PL spectra. It happens because of the decrease in oxygen vacancies behaving as shallow donors when the ambient oxygen pressure increases during thin films growth supply.

Figure 6(a) shows the emergence of emission peaks with the decrease in temperature in cobalt-doped ZnO thin film. PL spectra for copper-doped ZnO and undoped ZnO thin film samples obtained at low temperature (10 K) being compared in Fig. 6(b). Two dominant peaks appear around 3.357 and 3.312 eV were observed in PL spectrum of undoped ZnO film, shown in Fig. 6(b). On the basis of peak position it is assumed that the emission line appearing at 3.36 eV is due to neutral donor bound exciton (D⁰X) complex, the other dominant peak appearing around 3.33 eV is expected because of two-electron satellite (TES) recombination line of the D⁰X. The difference between D⁰X and TES is about 30 meV, which is well in agreement with the reported values for D⁰X and TES appearing in ZnO [22]. PL spectra measured at low temperature for copper-doped ZnO thin films exhibit weak donor bound exciton (D⁰X) emissions appearing around 3.36 eV as compared to ZnO followed by FE emissions at 3.37 eV towards higher energy side of spec-

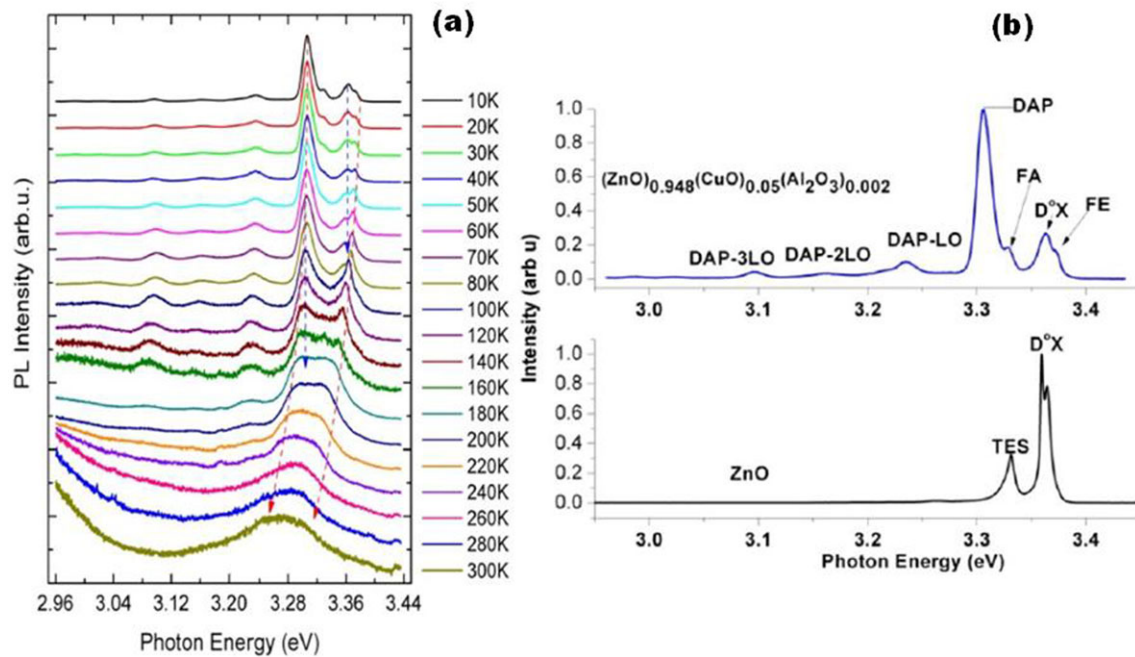


Fig. 6 (a) Low-temperature PL spectra for thin films grown in 1×10^{-2} mbar O_2 . (b) Different emissions appear at low temperature

trum. Furthermore, few peaks appearing around 3.30, 3.23, 3.16 and 3.09 eV indicate an enhancement in optical quality of thin films [23]. In copper-doped ZnO thin film, emission peak appears at 3.30 eV, becoming clearly distinguishable with decreasing temperature (at about 120 K) shown in Fig. 6(a). Emission peak at 3.30 eV is expected due to acceptor-related transitions like free electron to neutral acceptor (FA) and donor-acceptor-pair (DAP) [24–26]. In DAP transition, some electrons of neutral donors combine with holes of neutral acceptors and emit luminescence. The defect binding energy for a donor lies between 5–50 meV and for acceptor lies between 20–200 meV depending on the nature of material [23]. The thermal energy can be compared to the donor binding energy when the temperature is higher, because electrons can easily cause ionization and DAP transition can be replaced by free electron to acceptor (FA). However, in our case, we see the FA emissions appear around 3.32 eV and DAP emission around 3.30 eV. By comparing the series of peaks at 3.30, 3.23, 3.16 and 3.09 eV, the most obvious difference is seen for the peak that appears at 3.30 eV, which has stronger line, others emission are weaker having broad lines centered at 3.23, 3.16, and 3.09 eV. It is seen that the emission peak of 3.30 eV shows a blue-shift with increasing excitation intensity; it can be attributed to a DAP transition [27]. Three small shoulders appearing towards lower-energy side from DAP transitions are given names as DAP-LO, DAP-2LO and DAP-3LO, respectively, the difference in the energy of peak positions is similar to LO phonon energy of ZnO. FA emission which is dependent on temperature can be used to calculate the accep-

tor binding energy using the following equation: $E_{FA}(T) = E_g(T) - E_A + k_B T/2$, where $E_g(T)$ and E_A are the bandgap energy and acceptor energy, respectively. The Varshni equation shows that the bandgap energy of ZnO has temperature dependence [27, 28], $E_g(T) = E_g(0) - \alpha T^2/(T + \beta)$, where $\alpha = 8.2 \times 10^{-4}$ eV K $^{-1}$, $\beta = 700$ K and $E_g(0) = 3.44$ eV [26, 29]. Based on the above mentioned values, the estimated acceptor energy (E_A) is 135 meV, which is reasonable compared with the estimated range of energy values, 120–200 meV.

Raman spectra of thin film samples showed the influence of Cu doping in ZnO via the change in Raman modes of ZnO for all the ZnCuAlO samples grown in different oxygen ambient pressures. ZnO has a wurtzite structure with P63mc point group symmetry. It was predicted on the basis of group theory that there are two A_1 , two E_1 , two E_2 and two B_1 modes in the Raman spectra of ZnO [19, 30]. We obtained E_2 modes in our samples along with additional modes and some modes belong to the sapphire substrates. A comparative study was done to see whether the additional modes (AMs) appear in Raman spectra of Cu doped ZnO films or not, on the other hand these modes appear in undoped ZnO thin film samples deposited under same ambient conditions, graphs are shown in Fig. 7(a). The peak appearing at 99 cm^{-1} represents E_2 (low) mode, while the peak at 437 cm^{-1} represents E_2 (high) mode for copper-doped ZnO thin films. The peaks appearing at 577 cm^{-1} are attributed to additional modes, also known as defect-induced modes [19]. The appearance of E_2 (high) is a symbol of wurtzite phase of ZnO [19]. It can be seen in

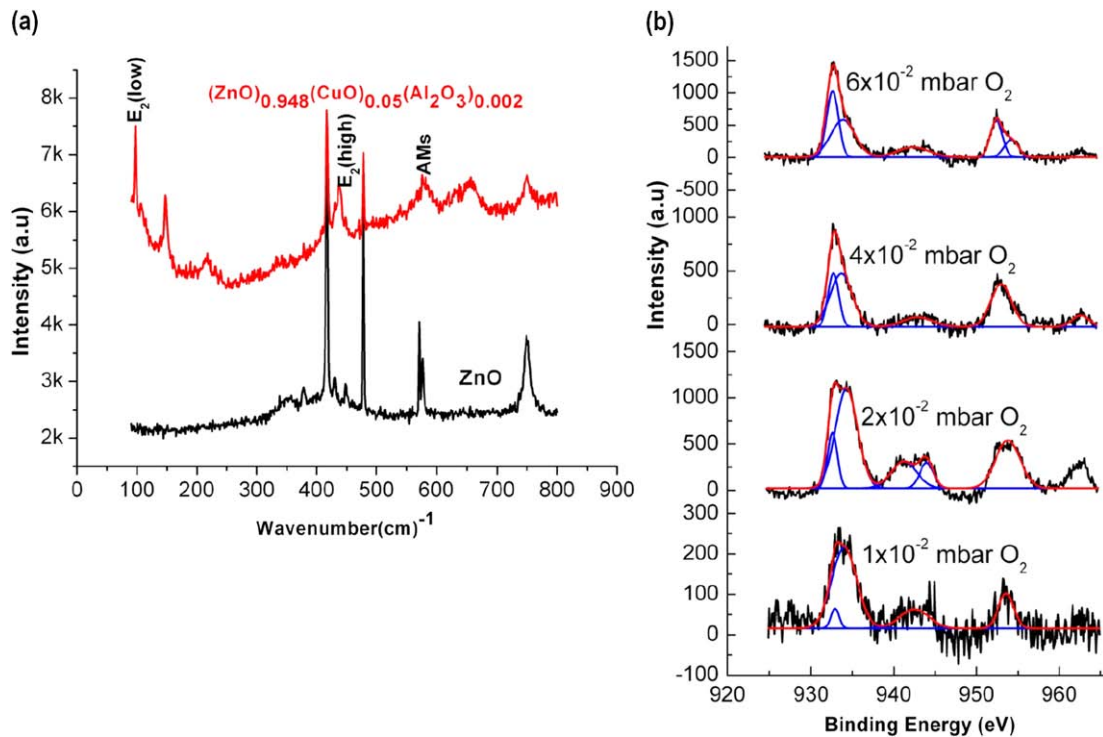


Fig. 7 (a) Raman spectra for the films grown in 2×10^{-2} mbar O_2 . (b) Cu 2p core peak spectra for thin films grown in different oxygen ambient pressures

Fig. 7(a) that the E_2 (high) mode has higher intensity in Cu doped thin film sample as compared to undoped ZnO increase in intensity showing improved crystalline quality of the ZnO film with Cu doping. Also the appearance of additional modes (defect-induced modes) at 577 cm^{-1} (denoted by AM1) is lower in intensity hinting toward minimum defects, i.e. better crystalline quality, in Cu doped ZnO thin films.

XPS was used to measure to obtain information about different valence states, Fermi energy level and valence-band maximum in thin films. For Zn 2p core peaks, binding energy (BE) values show a slight change as compared to bulk ZnO reference (1021.4 eV). The Zn $2p_{3/2}$ peak shows the BEs of 1021.8, 1021.4, 1021.6 and 1021.4 eV and Zn $2p_{1/2}$ peak shows the BEs of 1044.9, 1044.5, 1044.7 and 1044.5 eV for thin film samples grown at oxygen ambient pressures of 1×10^{-2} , 2×10^{-2} , 4×10^{-2} and 6×10^{-2} mbar, respectively. A high resolution scan was done to get core peak spectra of Cu 2p peaks. A detailed scan is helpful to understand the bonding nature of oxygen atoms with copper atoms substituted at Zn sites in the film shown in Fig. 7(b). XPS core peak spectrum clearly differentiates between oxidation states of Cu i.e. Cu^{2+} and Cu^{1+} , Cu^{2+} is expected to produce satellite peaks towards higher binding energy side, and the appearance of satellite peaks indicates the presence of 3d hole states of Cu; in case of Cu^0 and Cu^{1+} not any satellite peak is expected [9]. The de-

convolution of the peaks that appear at 933.8, 933.8, 932.6 and 932.9 eV for thin films samples grown at 1, 2, 4 and 6×10^{-2} mbar O_2 was done. The deconvolution of peaks clearly shows the +2 oxidation state because of the appearance of peaks at BE values of 934.01, 934.28, 933.65 and 933.85 eV for each of the different samples. Satellite peak of Cu 2p shows Cu^{2+} presence, but this satellite position varied with atomic environment of Cu^{2+} . It is expected that there appears a very weak satellite peak of Cu^{2+} around 943 eV. The area of satellite peak of Cu at 943 eV becomes wider with the increase in ambient oxygen pressure [31]. The change in valence band is 0.90, 1.53, 1.89 and 2.20 eV for thin films deposited in 1×10^{-2} , 2×10^{-2} , 4×10^{-2} , 6×10^{-2} mbar oxygen pressure, respectively. The valence-band (VB) spectra, obtained from XPS, for copper-doped ZnO samples grown are shown in Fig. 8(a).

As shown in Fig. 8(a), the weak peaks around Fermi level, E_F , are a kind of non-local states in the bandgap possibly caused by defects. Peaks observed around 4.6, 4.33, 3.97 and 4.11 eV for thin films grown at 1×10^{-2} , 2×10^{-2} , 4×10^{-2} and 6×10^{-2} mbar O_2 pressure showed involvement of O 2p orbitals, O 2p and Zn 4s orbitals hybridized with each other. Peaks observed around 9.98, 9.97, 10.12 and 10.03 eV, respectively, are expected due to the Zn 3d band. The shift in the binding energy is seen with the variation in the oxygen pressure inside the chamber. In peak regions of O 2p, the uppermost valence-band edges (VBE),

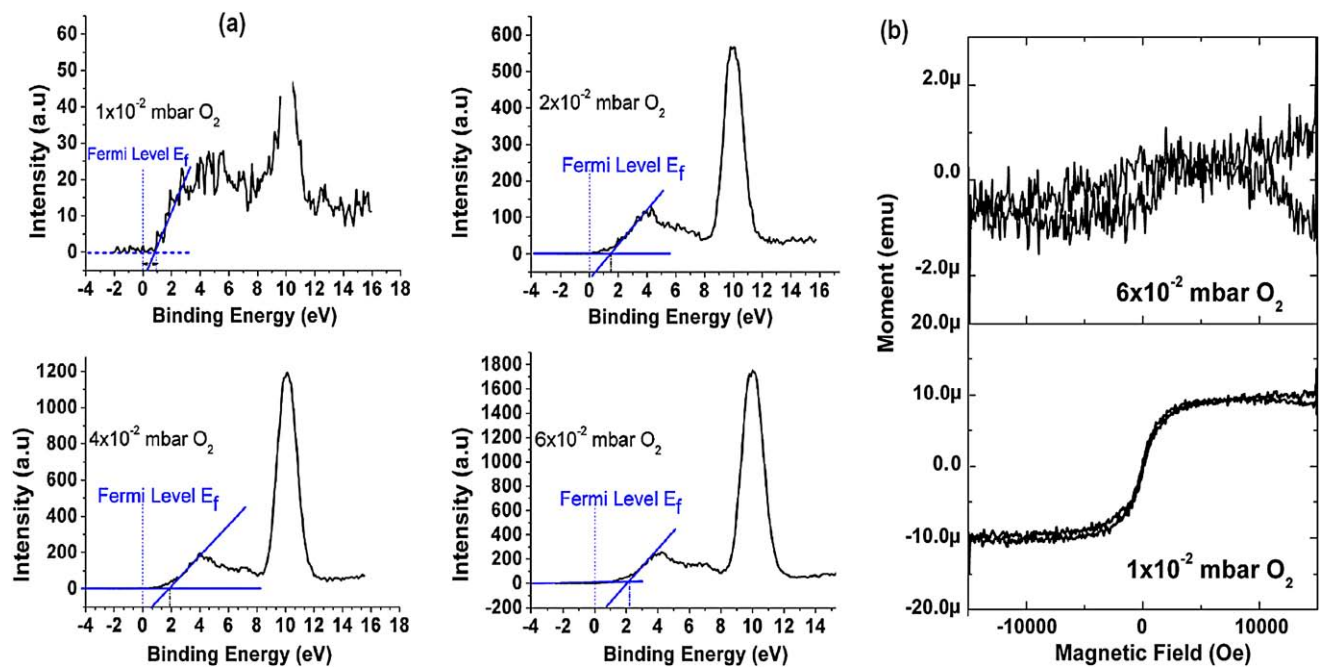


Fig. 8 (a) Valence-band spectra for $(\text{ZnO})_{0.948}(\text{CuO})_{0.05}(\text{Al}_2\text{O}_3)_{0.002}$ thin films in different O_2 pressures. (b) Hysteresis curves for $(\text{ZnO})_{0.948}(\text{CuO})_{0.05}(\text{Al}_2\text{O}_3)_{0.002}$ thin films

could be easily separated out. The VBE was linearly fitted to determine the shift, ΔE_v , as shown by diagonal lines in Fig. 8(a). The tangents to the fitted curves were drawn and their intersect is defined as VBM [32]. It is evident from Fig. 8(a) that the VBM of thin films shifts towards higher binding energy by increasing the oxygen pressure. It shows that the oxygen partial pressure affects the valence-band position.

The magnetic characterizations at room temperature show a weakly expressed ferromagnetic ordering in thin films deposited at oxygen pressure of 1×10^{-2} mbar, shown in Fig. 8(b). On the other hand, the films grown in oxygen ambient pressure of 6×10^{-2} mbar show no ferromagnetism. Experimentally, the O_2 partial pressure is an important factor in the magnetic behavior of the material. The main donor defects which induce ferromagnetism arise in thin films when deposited in low oxygen pressure [33]. The oxygen vacancies defect is necessary to induce ferromagnetic coupling. Thin films deposited for 5 % Cu doped ZnO gives magnetic behavior in low oxygen pressure (1×10^{-2} mbar), while the magnetic behavior vanished in higher ambient pressures of oxygen (6×10^{-2} mbar) during the film growth, which hints towards the decrease in donor defects.

3 Conclusion

A detailed study on copper-doped ZnO system was done, bulk and thin films of copper-doped ZnO system showed

ferromagnetism. Detailed XPS analyses were done on the surface of bulk samples, which indicate the +1 and +2 oxidation states of copper ions. After the detailed characterization of the bulk samples, thin film samples were deposited on sapphire substrates in vacuum using pellets with different Cu doping percentages. The preferred orientation in thin films was found to be along the (002) plane of ZnO. XPS analyses of films indicate different oxidation states of dopants, the dominant oxidation state of Cu dopant which is +2 is expected to contribute to the magnetic behavior of thin film samples. $M-H$ graphs give weak ferromagnetic content for 1–3 % Cu doping but for 5 % Cu doped thin film sample showed the diamagnetic behavior. Another set of thin film samples were grown for 5 % Cu doped ZnO bulk pellet in different oxygen ambient pressures. The preferred orientation in thin films is along the (002) plane of ZnO. Raman spectra showed a weak signal for thin film samples. Low-temperature PL spectra show peak emergence at 3.30 eV, which is due to acceptor-related transitions. XPS results show that copper exists in Cu^{2+} and Cu^{+1} valence states. The valence-band maximum of thin films shifts towards higher binding energy with increasing oxygen pressure. Furthermore, hysteresis curves showed the ferromagnetism only for the thin films sample grown at low oxygen pressure (1×10^{-2} mbar), while the magnetic behavior vanished for the film grown at higher ambient pressures of oxygen (6×10^{-2} mbar), which hints towards the decrease in donor defects.

References

1. Zutic, I., Fabian, J., Das Sarma, S.: *Rev. Mod. Phys.* **76**, 323 (2004)
2. Binasch, G., Grunberg, P., Saurenbach, F., Zinn, W.: *Phys. Rev. B* **39**, 4828 (1989)
3. Baibich, M.N., Broto, J.M., Fert, A., Nguyen van Dau, F., Petroff, F., Eitenne, P., Creuzet, G., Friedrich, A., Chazelas, J.: *Phys. Rev. Lett.* **61**, 2472 (1988)
4. Schmidt, G., Ferrand, D., Molenkamp, L.W., Filip, A.T., van Wees, B.J.: *Phys. Rev. B* **62**, R4790 (2000)
5. Johnson, M., Silsbee, R.H.: *Phys. Rev. B* **35**, 4959 (1987)
6. Jonker, B.T., Erwin, S.C., Petrou, A., Petukhov, A.G.: *Mater. Res. Soc. Bull.* **28**, 740 (2003)
7. Ohno, H.: *Science* **281**, 951 (1998)
8. Feng, X.: *J. Phys. Condens. Matter* **16**, 4251 (2004)
9. Chakraborti, D., Narayan, J., Prater, J.T.: *Appl. Phys. Lett.* **90**, 062504 (2007)
10. Gupta, R.K., Ghosh, K., Patel, R., Mishra, S.R., Kahol, P.K.: *J. Cryst. Growth* **310**, 3019 (2008)
11. Khranovskyy, V., Grossner, U., Nilsen, O., Lazorenko, V., Lashkarev, G.V., Svensson, B.G., Yakimova, R.: *Thin Solid Films* **515**, 472 (2006)
12. Chien, C.H., Chiou, S.H., Gao, G.Y., Yao, Y.D.: *J. Magn. Magn. Mater.* **282**, 275 (2004)
13. Cho, C.H., Hwang, J.Y., Kim, J.P., Jeong, S.Y., Jang, M.S., Lee, W.J., Kim, D.H.: *Jpn. J. Appl. Phys.* **43**, L1383 (2004)
14. Amirhaghi, S., Craciun, V., Craciun, D., Elder, J., Boyd, I.W.: *Microwelectron. Eng.* **25**, 321 (1994)
15. Ohshima, T., Thareja, R.K., Ikegami, T., Ebihara, K.: *Surf. Coat. Technol.* **169–170**, 517 (2003)
16. Engin, M., Atay, F., Kose, S., Bilgin, V., Akyuz, I.: *J. Electron. Mater.* **38**, 786 (2009)
17. Mamazza, R. Jr., Morel, D.L., Ferekides, C.S.: *Thin Solid Films* **484**, 26 (2005)
18. Ferro, R., Rodriguez, J.A., Vigil, O., Morales-Acevedo, A.: *Mater. Sci. Eng. B* **87**, 83 (2001)
19. Wang, X.B., Song, C., Geng, K.W., Zeng, F., Pan, F.: *Appl. Surf. Sci.* **253**, 6905 (2007)
20. Hopfield, J.J., Thomas, D.G.: *Phys. Rev.* **122**, 35 (1961)
21. Reynolds, D.C., Look, D.C., Jobai, B., Litton, C.W., Collins, T.C., Harsch, W., Cantwell, G.: *Phys. Rev. B* **57**, 12151 (1998)
22. Wang, J.Z., Elamurugu, E., Sallet, V., Jomard, F., Lusson, A., Botelho do Rego, A.M., Barquinha, P., Goncalves, G., Martins, R., Fortunato, E.: *Appl. Surf. Sci.* **254**, 7178 (2008)
23. Wang, H., Ho, H.P., Lo, K.C., Cheah, K.W.: *J. Phys. D, Appl. Phys.* **40**, 4682 (2007)
24. Nakagawa, A., Masuoka, F., Chiba, S., Endo, H., Meguro, K., Kashiwaba, Y., Ojima, T., Aota, K., Niikura, I., Kashiwaba, Y.: *Appl. Surf. Sci.* **254**, 164 (2007)
25. Almamun Ashrafi, A.B.M., Suemune, I., Kumano, H., Tanaka, S.: *Jpn. J. Appl. Phys.* **41**, L1281 (2002)
26. Park, S., Minegishi, T., Oh, D., Lee, H., Taishi, T., Park, J., Jung, M., Chang, J., Im, I., Ha, J., Hong, S., Yonenaga, I., Chikyow, T., Yao, T.: *Appl. Phys. Express* **3**, 031103 (2010)
27. Sun, J.W., Lu, Y.M., Liu, Y.C., Shen, D.Z., Zhang, Z.Z., Yao, B., Li, B.H., Zhang, J.Y., Zhao, D.X., Fan, X.W.: *J. Appl. Phys.* **102**, 043522 (2007)
28. Wang, L.J., Giles, N.C.: *Appl. Phys. Lett.* **84**, 3049 (2004)
29. Lu, J., Liang, Q., Zhang, Y., Ye, Z., Fujita, S.: *J. Phys. D* **40**, 3177 (2007)
30. Damen, T.C., Porto, S.P.S., Tell, B.: *Phys. Rev.* **142**, 570 (1966)
31. Leea, J.B., Leea, H.J., Seob, S.-H., Parka, J.S.: *Thin Solid Films* **398–399**, 641 (2001)
32. Joshi, A.G., Sahai, S., Gandhi, N., Radha Krishna, Y.G., Haranath, D.: *Appl. Phys. Lett.* **96**, 123102 (2010)
33. Liu, X.C., Shi, E.-W., Chen, Z.Z., Chen, B.Y., Zhang, T., Song, L.X., Zhou, K.J., Cui, M.Q., Yan, W.S., Xie, Z., He, B., Wei, S.Q.: *J. Phys. Condens. Matter* **20**, 025208 (2008)